communications chemistry

A Nature Portfolio journal

Article

https://doi.org/10.1038/s42004-026-01933-8

Scaffold-client behavior and structural organization in multicomponent protein condensates as revealed by studying tau/TDP-43 droplets

Vitor Ulisses Monnaka [1,2], Brandon Shipley[3], Solomiia Boyko[2], Patricia Maria de Carvalho Aguiar [1,4], Michael Hinczewski [3,4] ✉ & Witold K. Surewicz [2,4] ✉

Liquid-liquid phase separation (LLPS) is known to modulate pathological aggregation of proteins implicated in neurodegenerative diseases, such as tau and TDP-43. While LLPS mechanisms of individual proteins are well characterized, much less is known about phase behavior of multicomponent protein systems. Here, we investigated the LLPS behavior of mixtures of tau and TDP-43 low complexity domain (LCD), two proteins known to co-aggregate in Alzheimer's disease. We found that, depending on the concentration, each protein can function either as a scaffold (driving condensate formation) or as a client (passively recruited into condensates formed by the other). Notably, scaffold-client roles can be modulated by selectively inhibiting the interactions driving LLPS: electrostatic for tau, and hydrophobic for TDP-43 LCD. A striking feature of this system is the formation of a tau "halo" around TDP-43 LCD droplets, which coarse-grained simulations reveal to arise from tau's amphiphilic organization at condensate interfaces. Together, these findings provide molecular-level insights into the general principles governing the assembly and organization of multicomponent protein condensates.

Liquid-liquid phase separation (LLPS) occurs when multivalent interactions between macromolecules are stronger than those with the solvent, driving the transition of a homogeneous solution into coexisting dense and dilute phases[1]. Although LLPS has long been studied in polymer chemistry, its biological relevance has only recently been fully recognized upon realization that phase separation of proteins and nucleic acids underlies the formation of membrane-less organelles (MLOs)[2–4]. These dynamic assemblies compartmentalize biochemical reactions throughout the cytoplasm and nucleus, playing a central role in cellular biology[5,6]. Beyond its physiological functions, LLPS has been increasingly implicated in the pathogenesis of several diseases, particularly neurodegenerative disorders such as Alzheimer's diseases, amyotrophic lateral sclerosis and frontotemporal dementia, where it appears to modulate the formation of pathological protein aggregates[7–9].

The mechanisms by which individual proteins undergo LLPS are relatively well understood[10,11]. These proteins often contain intrinsically disordered regions, often of low sequence complexity, which lack stable three-dimensional structure and behave as simple polymers in solutions, forming dynamic networks of multivalent interactions[12,13]. In contrast, biologically relevant MLOs comprise large numbers of proteins, and our understanding of the principles governing phase behavior in such multicomponent systems remains limited. Typically, only a small subset of these proteins — called scaffolds — is essential for condensate formation, while many others — referred to as clients — are passively recruited into the condensate interior[14–16]. Strong heterotypic interactions between scaffolds tend to drive associative LLPS, resulting in a homogeneous molecular distribution within condensates[17,18]. Conversely, weak heterotypic interactions promote non-associative LLPS, leading to multiphase structures in which condensates with higher surface tension localize within the core of more hydrophilic droplets[19–22]. However, a homogeneous distribution of proteins within condensates can also arise when scaffolds recruit proteins that are unable to undergo LLPS on their own (e.g., at low concentrations), even in the absence of strong heterotypic interactions[21]. Therefore, determining whether such uniform distribution reflects true associative behavior or

[1]Faculdade Israelita de Ciências da Saúde Albert Einstein, Hospital Israelita Albert Einstein, São Paulo, Brazil. [2]Department of Physiology and Biophysics, Case Western Reserve University, Cleveland, OH, USA. [3]Department of Physics, Case Western Reserve University, Cleveland, OH, USA. [4]These authors jointly supervised this work : Patricia Maria de Carvalho Aguiar, Michael Hinczewski, Witold K. Surewicz. ✉e-mail: mxh605@case.edu; wks3@case.edu

passive client recruitment requires knowledge of each protein's intrinsic propensity to phase separate in multicomponent systems.

Understanding the LLPS behavior of multicomponent protein systems is particularly critical in the context of neurodegeneration, where liquid condensates often act as intermediate states along the protein aggregation pathway[23–26]. While these diseases have been traditionally linked to aggregation of single protein species — such as tau in tauopathies and TDP-43 in TDP-43 proteinopathies — emerging evidence indicates considerable pathological overlap between these disorders[27]. Notably, tau and TDP-43, two LLPS-prone proteins, have been found to colocalize in toxic aggregates in post-mortem brains of individuals with Alzheimer's disease and cerebral age-related TDP-43 with sclerosis[28,29]. These observations highlight the prevalence of mixed proteinopathies in aging individuals[30] and suggest that distinct disease-associated proteins may interact synergistically during aggregation.

Given the major role of LLPS in the aggregation of many proteins, here we focused on gaining detailed molecular level understanding on the LLPS behavior of a mixture of tau and the low-complexity C-terminal domain of TDP-43 (TDP-43 LCD). This domain is of particular interest, as it drives both phase separation and aggregation of the full-length TDP-43[31,32]. Beyond its disease relevance, tau/TDP-43 LCD system offers a uniquely suitable model for studying the general principles governing formation and properties of multicomponent protein condensates. This is because LLPS of tau and TDP-43 LCD is driven by fundamentally different interaction types[31,33–35], and these distinct interactions can be selectively modulated in a well-controlled manner.

Results

The scaffold-client behavior of tau and TDP-43 LCD mixture is controlled by relative concentration of both proteins

Before exploring the LLPS behavior of tau/TDP-43 LCD mixtures, we first determined saturation concentrations (C_{sat}) of these proteins individually, i.e., the concentrations above which they undergo LLPS[36]. These experiments were performed in 10 mM HEPES buffer (pH 7.4) containing 150 mM NaCl, 1 mM DTT and 1 mM EDTA. Since tau requires the presence of crowding agents to undergo LLPS at physiologically relevant concentrations[33], 10% polyethylene glycol 10 (PEG) was used in all experiments described in this study. Using turbidimetry measurements, we found the saturation concentration of tau and TDP-43 LCD under the above-mentioned buffer conditions to be 4.9 μM and 4.8 μM, respectively (Fig. 1a). The absence of droplets below C_{sat}, and their presence above C_{sat}, was confirmed by fluorescence microscopy using tau labeled with Alexa Fluor 488 (green) and TDP-43 LCD labeled with Alexa Fluor 594 (red) (Fig. 1b).

The C_{sat} determined in this study for tau is consistent with the previously reported phase diagrams that placed the threshold concentration for tau LLPS under identical buffer conditions (150 mM Nacl, 10% PEG, pH 7.4) between 4 and 5 μM[37,38]. While a range of C_{sat} values were reported for TDP-43, some of them were determined for the full-length protein and/or under different buffer conditions[39,40]. The C_{sat} value previously determined for TDP-43 LCD at a similar ionic strength (150 mM NaCl) in the absence of any molecular crowders was around 15 μM[32,41,42]. Thus, while PEG decreases the C_{sat} of TDP-43 LCD from 15 μM to 4.8 μM, its promoting effect on tau LLPS is stronger, as the latter protein in the absence of crowding agents does not undergo phase separation even at concentrations as high as 100 μM[33]. In view of these data, we performed control experiments exploring whether there is any specific interaction between PEG and any of the two proteins used. Using fluorescenly labeled PEG, we found that this polymer does not partition into tau or TDP-43 LCD droplets (Fig. S1). This indicates that in our system PEG acts as an inert crowding agent that does not interact specifically with any of the proteins used[43].

We began by characterizing the phase behavior of tau/TDP-43 LCD mixture under the conditions where both proteins were above their respective saturation concentrations. Droplets formed by these two proteins were found to be immiscible, with relatively small TDP-43 LCD condensates engulfed by larger tau droplets, typically residing close to the inner surface of the latter (Fig. 2a, b). Notably, tau was present not only within these larger droplets but was also recruited into the smaller TDP-43 LCD condensates, as indicated by fluorescence intensity profiles (Fig. 2 a, b, right panels). Furthermore, an important feature of this three-phase system was that tau accumulated at especially high concentration at the surface of TDP-43 LCD droplets, forming a halo around them. We also assessed whether all tau droplets exhibit a heterotypic character, defined as containing TDP-43 LCD at intensities exceeding a defined detection threshold. To this end, we quantified mean TDP-43 LCD fluorescence intensities within the regions corresponding to each tau condensate in a representative 100 × 75 μm field (Fig. S2a). All 65 condensates displayed TDP-43 LCD intensities markedly above those of the surrounding dilute phase, indicating that every tau droplet contained detectable TDP-43 LCD under these conditions. The segmentation procedure and criteria used to define the TDP-43 LCD detection threshold are detailed in the Methods section.

Next, we explored whether each of these two proteins below its saturation concentration (i.e., when alone it did not undergo LLPS) could be recruited into droplets formed by the other protein. When tau at 4 μM (below C_{sat}) was mixed with TDP-43 LCD at 20 μM (above C_{sat}), it was robustly recruited into TDP-43 LCD droplets, as clearly indicated by fluorescence microscopy images and fluorescence intensity profile (Fig. 2c). Importantly, akin to the situation observed for TDP-43 LCD condensates engulfed by tau droplets (Fig. 2a, b), tau was especially highly concentrated at the surface of TDP-43 LCD droplets (Fig. 2c). A similar recruitment of TDP-43 LCD into tau condensates was observed when the latter protein below its C_{sat} was mixed with tau above its C_{sat} (Fig. 2d). However, in this case the distribution of both proteins was uniform within tau droplets, with no halo effect observed. Akin to the situation when both proteins were above C_{sat}, all condensates under this regime were also heterotypic (Fig. S2b).

We also performed limited experiments in the absence of PEG, finding that, also in this case, tau (which does not undergo LLPS under these conditions) could be recruited into TDP-43 LCD droplets (Fig. S3). However, no detectable halo effect was observed in this case, suggesting that accumulation of tau molecules at the surface of TDP-43 LCD droplets is especially strongly promoted by crowding conditions.

To confirm that these proteins are recruited into each other's condensates only as passive clients and not through a synergistic LLPS-promoting interaction, we mixed both proteins in a PEG-containing buffer at 4 μM each, resulting in a cumulative concentration (8 μM) that exceeded the C_{sat} of each protein individually. No droplets were observed under these conditions (Fig. S4a), indicating that heterotopic interactions between tau and TDP-43 LCD are not sufficient to drive phase separation. This conclusion is further supported by turbidity measurements showing no detectable increase in optical density in the presence of the mixture of tau and TDP-43 LCD at 4 μM each, in contrast to elevated turbidity when either of these proteins is present alone at a concentration of 5 μM or higher (Fig. S4b).

Altogether, these findings demonstrate that the scaffold-client behavior of the tau/TDP-43 LCD mixture is controlled by the relative concentration of these proteins, and that each of them can behave either as a scaffold that drives LLPS (when above C_{sat}) or a passive client recruited into droplets formed by the other protein (when below C_{sat}).

Surface tension differences determine the overall multiphase architecture of tau/TDP-43 LCD droplets

Previous studies indicate that the organization of multiphase condensates is primarily governed by differences in surface tension between constituent phases[19–21]. When two immiscible condensates coexist, the phase with lower surface tension relative to the solvent tends to envelop the one with higher surface tension, thereby minimizing the total interfacial free energy. A commonly used approach to explore this issue is to characterize the wetting behavior of individual condensates on polar surfaces, as this behavior has been shown to correlate with hierarchical organization of these condensates in multiphasic systems: droplets that spread more extensively (lower

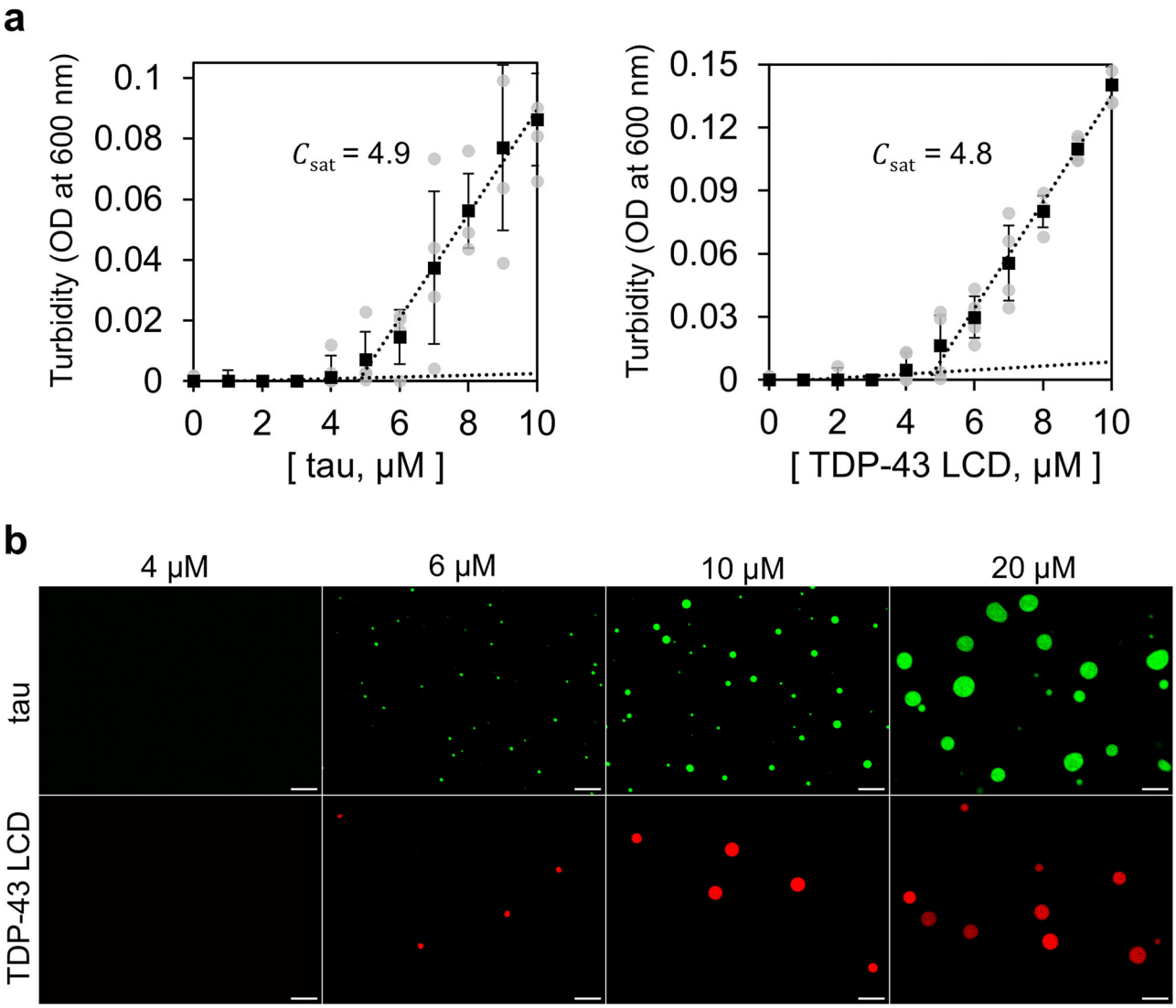

Fig. 1 | Liquid–liquid phase separation of tau and TDP-43 LCD individually. **a** Determination of saturation concentrations (C_{sat}) for LLPS of tau and TDP-43 LCD. Turbidity (OD at 600 nm) was measured as a function of protein concentration. C_{sat} values correspond to the intersection points of the linear fits applied to the data. Gray circles show individual measurements; black squares indicate the mean, and error bars represent the standard deviation ($n = 4$ experimental replicates). **b** Fluorescence microscopy images of tau (green) and TDP-43 LCD (red) at the indicated protein concentrations. Scale bars: 5 μm.

interfacial angle) generally form the outer layers, whereas more hydrophobic droplets (higher contact angle) are encapsulated[20]. Therefore, to gain insight into the biophysical basis of multilayer architecture of tau/TDP-43 LCD droplets, we assessed the relative surface tension of droplets formed by each protein individually by measuring their interfacial angle on a polar glass surface[21]. The interfacial angle of tau droplets (~17°) was found to be markedly lower than that of TDP-43 LCD droplets (~53°), indicating substantially higher surface tension of the latter condensates (Fig. 2e). This difference explains why TDP-43 LCD droplets are engulfed by tau droplets, as such an arrangement is energetically more favorable, consistent with the wetting behavior observed in other multiphasic systems[19–21].

Material properties of tau and TDP-43 LCD condensates

To explore material properties of condensates under study, we performed fluorescence recovery after photobleaching (FRAP) measurements on droplets formed by each protein individually (20 μM) and in multiphasic condensates generated by their mixture (Fig. 3). Immediately after formation, both tau and TDP-43 LCD droplets individually as well as in the context of multiphasic condensates depicted in Fig. 2a, b exhibited a rapid and very substantial (higher than 80 and 75% for tau and TDP-43, respectively) recovery of fluorescence signal, indicating a dynamic, liquid-like nature of these condensates. After 24 h, however, TDP-43 LCD droplets alone as well as within mixed condensates displayed markedly reduced fluorescence recovery, indicating a transition toward a more solid-like state. In contrast, consistent with the previous study[37], tau condensates alone showed little aging, remaining highly dynamic even after 24 h incubation. However, a partial loss of fluorescence recovery was observed after 24 h for tau molecules within multiphasic condensates. This indicates restricted mobility of these molecules, likely due to their interactions with "solidified" TDP-43 molecules.

Modulation of the scaffold-client behavior of tau/TDP-43 LCD mixture by selective inhibition of intermolecular interactions

Next, we aimed to determine the role of specific intermolecular interactions in the scaffold-client behavior of the tau/TDP-43 LCD mixture. These two proteins form condensates through distinct mechanisms: while LLPS of TDP-43 LCD is believed to be driven largely by hydrophobic interactions involving aromatic residues[35], the major driving forces for tau LLPS are attractive electrostatic interactions between oppositely charged domains[33]. Therefore, this system allows protein-specific inhibition of LLPS driving

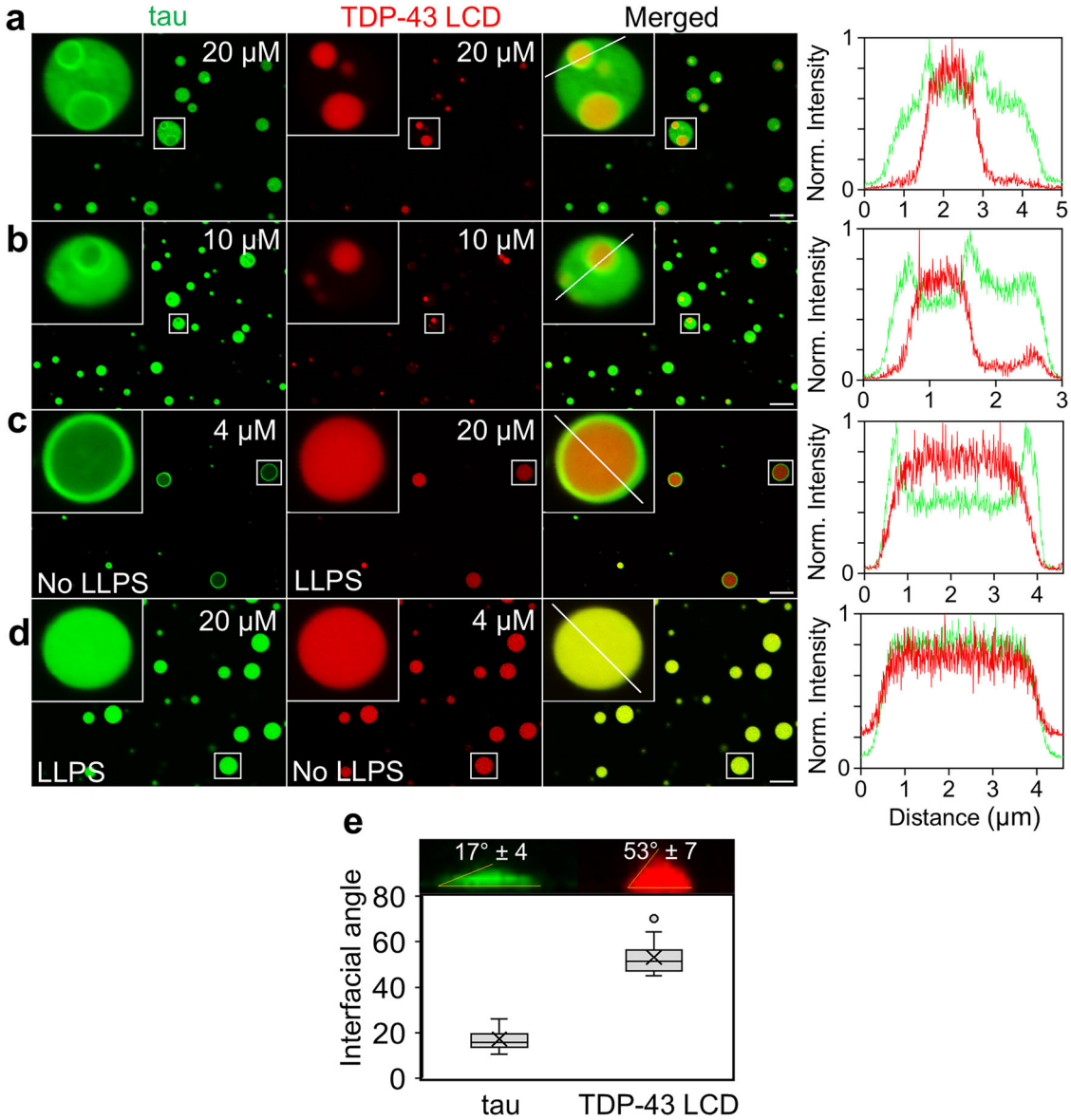

Fig. 2 | Phase behavior of tau and TDP-43 LCD mixtures. a–d Fluorescence microscopy images of tau (green) and TDP-43 LCD (red) mixtures at the indicated protein concentrations. Insets in the upper left corners show magnified view of selected droplets. Scale bars: 5 μm. Right panels display fluorescence intensity profiles (normalized to the maximum intensity) along the lines indicated in the corresponding merged images. **e** Orthogonal fluorescence microscopy views of tau (green) and TDP-43 LCD (red) droplets sedimented on a polar glass surface (top). Boxplots (bottom) show the distribution of interfacial angles measured at the condensate-glass interface for each protein ($n = 15$). Mean and standard deviation of interfacial angles are indicated above droplets.

Fig. 3 | Material properties of tau and TDP-43 LCD condensates. Representative fluorescence recovery after photobleaching (FRAP) traces at 0 h and after 24 h incubation (20 μM each protein) for single-component condensates (tau, green, $n = 8$ at 0 h and $n = 6$ at 24 h; TDP-43 LCD, blue, $n = 6$ at 0 h and $n = 7$ at 24 h) and within multiphasic condensates (tau compartment, yellow, $n = 7$ at 0 h and $n = 4$ at 24 h; TDP-43 LCD compartment, black, $n = 7$ at 0 h and $n = 4$ at 24 h). Individual measurements are shown as lighter-colored circles, squares show the mean, and error bars represent standard deviation.

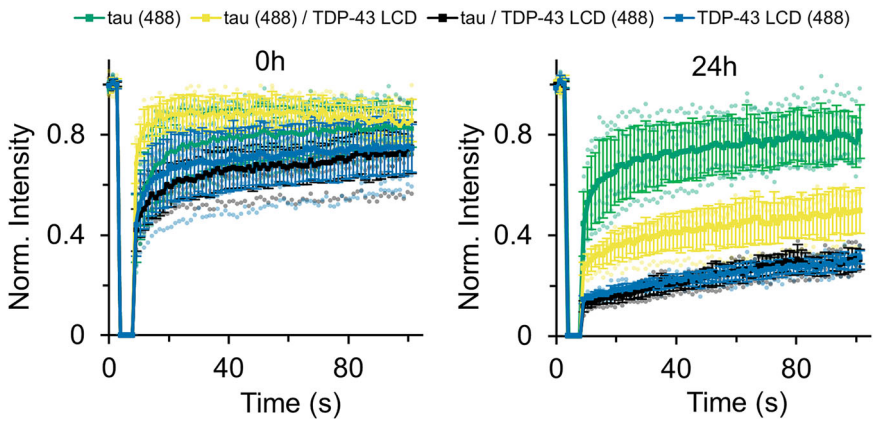

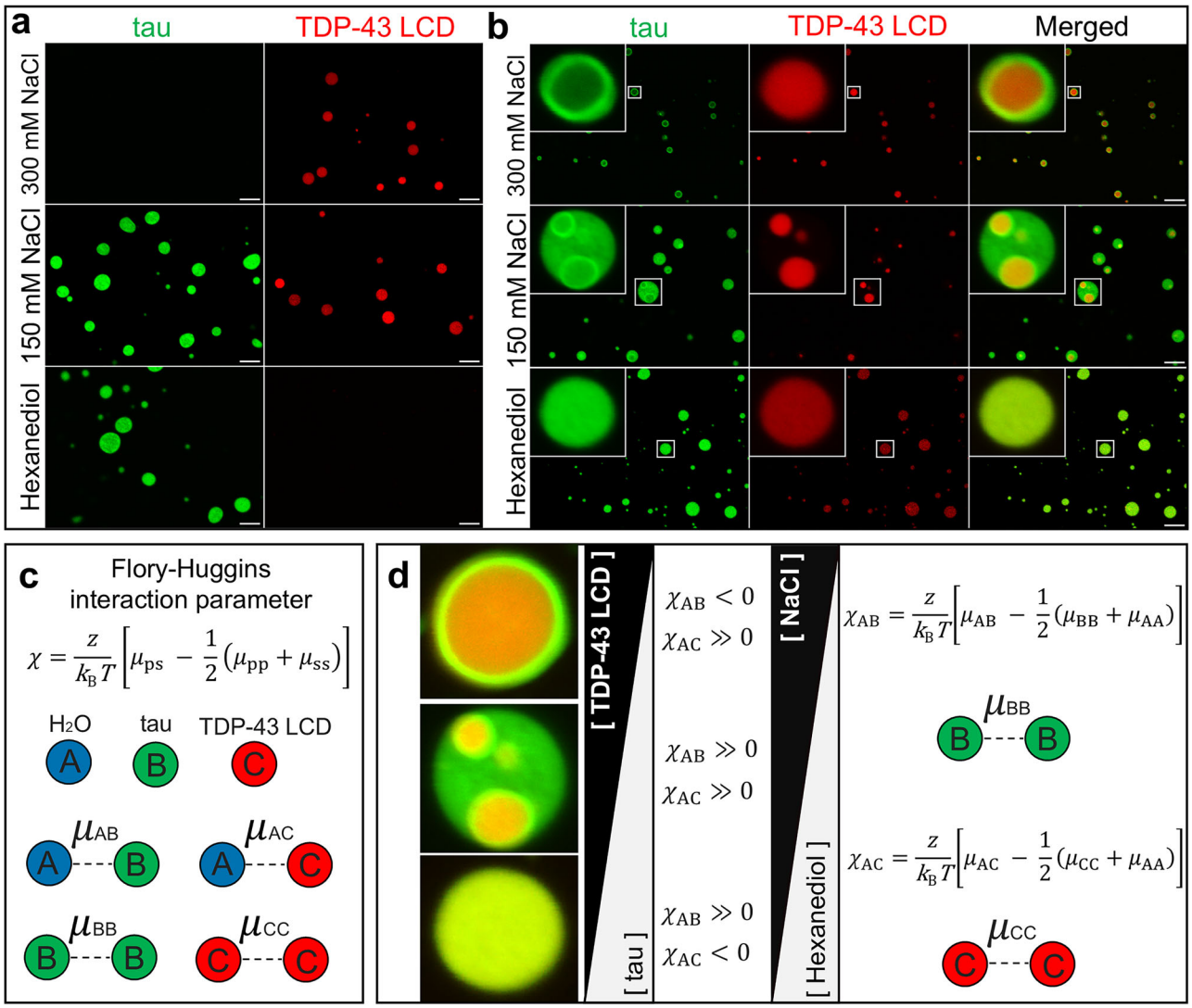

Fig. 4 | Selective inhibition of LLPS-driving interactions alters the scaffold-client behavior of tau/TDP-43 LCD mixture. a Fluorescence microscopy images of tau (green) and TDP-43 LCD (red) individually at 300 mM NaCl (*top*), 150 mM NaCl (*middle*), and 150 mM NaCl with 7.5% hexanediol (*bottom*). **b** Fluorescence microscopy images of tau (green) and TDP-43 LCD (red) (20 μM each) mixtures at 300 mM NaCl (*top*), 150 mM NaCl (*middle*), and 150 mM NaCl with 7.5% hexanediol (*bottom*). Scale bars: 5 μm. **c** Flory-Huggins interaction parameter (χ) and intermolecular interactions between the three components of our system (z, lattice site; k_BT, thermal energy; μ, mean-field energy; p, protein. s, solvent). **d** Flory-Huggins interaction parameter (χ) can be shifted to negative values either by reduction of protein concentration or inhibition of LLPS-driving interactions.

forces, offering unique opportunities in studying the mechanisms of multicomponent condensate formation.

We started by using 1,6-hexanediol, a compound known to inhibit LLPS of some proteins by interfering with hydrophobic interactions[44]. In control experiments with 20 μM of each protein, we found that 1,6-hexanediol at concentrations above 7.5% completely abrogated LLPS of TDP-43 LCD, whereas it had essentially no effect on tau condensation (Fig. 4a, bottom and Fig. S5a), consistent with the previous reports[31,33]. When 7.5% 1,6-hexanediol was added to the mixture of both proteins at physiological salt concentration, we no longer observed immiscible tau/TDP-43 LCD droplets that were present in the absence of 1,6-hexanediol (Fig. 4b, middle). Instead, TDP-43 LCD was recruited into tau droplets, where both proteins appeared to be evenly distributed (Fig. 4b, bottom), exactly as observed for the mixture of tau above its C_{sat} and TDP-43 LCD below its C_{sat} (Fig. 2d).

We followed this line of investigation by increasing salt concentration (in the absence of 1,6 hexanediol) to specifically inhibit electrostatic interactions. In control experiments with 20 μM of each protein, we established that TDP-43 LCD in the presence of 300 mM NaCl undergoes robust LLPS, whereas electrostatically driven LLPS of tau is completely abolished at this salt concentration (Fig. 4a, *top* and Fig. S5b). We next added increasing amounts of salt to the tau/TDP-43 LCD mixture (20 μM each), finding that increasing NaCl concentration from 150 to 300 mM completely changed the phase behavior of this system. Instead of forming immiscible droplets (as observed at 150 mM NaCl, Fig. 4b, *middle*), tau was now recruited into TDP-43 LCD droplets and highly concentrated at their surface (Fig. 4b, *top*), an arrangement essentially identical to that observed at lower salt concentrations for the mixture of TDP-43 LCD above its C_{sat} with tau below its C_{sat} (Fig. 2c). Collectively, these data demonstrate that inhibition of specific intermolecular interactions can control the phase separation behavior of the TDP-43 LCD/tau system.

The scaffold-client behavior observed in the tau/TDP-43 LCD mixture can be qualitatively explained within the general framework of the Flory-Huggins theory, which describes how molecular concentration and interaction strength govern phase behavior[12]. In this theory, the Flory-Huggins interaction parameter (χ) quantifies the energy of mixing resulting from the balance between protein-protein and protein-solvent interactions, as

illustrated schematically for our system in Fig. 4c. Phase separation becomes energetically favorable when protein-protein interactions are more favorable than protein-solvent interactions (i.e., $\chi > 0$). In the present study, we used this theory purely as a conceptual tool to qualitatively interpret our experimental observations, with no attempt to determine absolute thermodynamic parameters.

In our system, the Flory-Huggins interaction parameters for tau (χ_{AB}) and TDP-43 LCD (χ_{AC}) are negative when either of these proteins is below its respective C_{sat}, as LLPS-driving intermolecular interactions are infrequent at low protein concentration levels. Under such conditions, each protein can be recruited as a client into condensates formed by the other (if the latter is above C_{sat}). Conversely, when tau or TDP-43 LCD are above their respective C_{sat}, the corresponding χ becomes positive, and each protein undergoes LLPS independently, behaving as a scaffold. Importantly, our present data indicate that these interaction parameters can be shifted to negative values even at very high protein concentrations by selectively inhibiting specific intermolecular interactions driving phase separation. For instance, χ_{AC} becomes negative when hydrophobic interactions driving LLPS of TDP-43 LCD (μ_{CC}) are impaired by 1,6-hexanediol, while χ_{AB} becomes negative when electrostatic interactions driving tau LLPS (μ_{BB}) are inhibited at high ionic strength (Fig. 4d).

Altogether, these findings indicate that the phase behavior of multicomponent protein system can be modulated not only by protein concentration but also by selectively inhibiting specific LLPS-driving interactions. An important implication of this finding is that information about LLPS behavior of individual proteins may provide a foundation for understanding, and potentially predicting, the scaffold-client behavior of complex multicomponent systems.

Evaluating interactions responsible for reciprocal recruitment of tau and TDP-43 LCD into droplets formed by each other

In addition to forming a halo around TDP-43 LCD droplets, tau is also recruited to the interior of these condensates (Fig. 2a-c). This occurs when tau is both above and below C_{sat}. To better understand the chemical nature of interactions responsible for these effects, we examined the effect of salt on relative tau concentration within engulfed TDP-43 LCD condensates compared to that in the bulk of tau droplets. At 50 mM NaCl, tau fluorescence intensity within TDP-43 LCD condensates was significantly higher than in the surrounding tau phase, as shown by the plot profiles (Fig. 5). On the other hand, at 150 mM NaCl, tau intensity was comparable between these two regions. Additionally, at lower salt concentrations, we observed that TDP-43 LCD droplets engulfed within tau condensates were significantly smaller than those at higher NaCl concentrations, suggesting a reduced tendency to fuse. This decreased fusion propensity at low ionic strength likely reflects lower surface tension at the interface between tau and TDP-43 LCD condensates, consistent with apparently stronger TDP-43 LCD–tau interactions, as suggested by an enhanced tau recruitment at low NaCl concentrations.

A similar salt dependence for tau recruitment into TDP-43 LCD droplets was observed below tau's C_{sat} (Fig. 6a). In this case, we were able to directly determine tau's partition coefficient by measuring its relative concentration (as assessed by fluorescence intensity) within TDP-43 LCD droplets and in the dilute phase. This partition coefficient decreased with increasing salt concentration, dropping from ~11 at 150 mM to ~3 at 600 mM NaCl (Fig. 6b).

Evaluation of salt effect on TDP-43 LCD recruitment into tau droplets was not feasible due to high sensitivity of tau condensates to ionic strength. Instead, we tested whether 1,6-hexanediol affects the interactions mediating this process. Hexanediol is known to disrupt LLPS of many proteins, presumably by suppressing hydrophobic interactions[36,45]. To our surprise, this agent had no measurable effect on TDP-43 LCD partitioning into tau condensates (Fig. 6c, d).

Overall, these results suggest that the recruitment of tau into TDP-43 LCD condensates is driven primarily by ionic interactions. In addition to classical attractive electrostatic interactions between oppositely charged side chains, these may also include cation-π interactions, a likely scenario given high abundance of arginine/lysine residues in tau and aromatic residues in TDP-43 LCD. However, the persistence of tau halo around TDP-43 LCD condensates at 600 mM NaCl suggests that hydrophobic forces also contribute to stabilizing this structure, as electrostatic interactions are unlikely to play a significant role at such high ionic strength.

Coarse-grained simulations model for LLPS of the tau/TDP-43 LCD system

To gain molecular level insight into the interactions involved in phase separation of tau/TDP-43 LCD mixtures, we utilized a sequence-dependent coarse-grained simulation framework that explicitly models electrostatic and hydrophobic interactions, incorporating the LLPS-promoting effects of PEG by empirically scaling these forces, as detailed in the Methods and Supplementary Methods.

To validate the coarse-grained simulation framework, we conducted simulations of tau and TDP-43 LCD mixtures under three experimentally tested conditions: (i) Both proteins below C_{sat} (3 μM each); (ii) Tau above C_{sat} and TDP-43 LCD below C_{sat} (9 μM and 3 μM, respectively); and (iii) TDP-43 LCD above C_{sat} and tau below C_{sat} (3 μM and 9 μM, respectively). Under the first set of conditions, LLPS was not observed in our simulations, consistent with the experimental results (Fig. S4). In the second and third regimes, droplets containing both proteins were formed (Fig. S6), in agreement with experimental data showing reciprocal recruitment of tau and TDP-43 LCD into droplets formed by the other protein (Fig. 2c, d).

For the second regime (9 μM tau and 3 μM TDP-43 LCD), TDP-43 LCD was distributed approximately evenly throughout the interior of the condensates (Fig. S6a). In the third regime (3 μM tau and 9 μM TDP-43 LCD), tau was recruited into TDP-43 LCD condensates (Fig. S6b). Importantly, in this case, our simulations also successfully recapitulated the experimentally observed enrichment of tau at the surface of TDP-43 LCD droplets. Thus, the coarse-grained framework was able to recapitulate at the qualitative level the key features of condensates formed by the mixture of tau and TDP-43 LCD.

Insight from simulations into intermolecular interactions between tau and TDP-43 LCD

Next, we employed the coarse-grained simulation framework to analyze in detail the most interesting situation, in which tau is recruited into TDP-43 LCD droplets while also being enriched at the surface, forming a halo around them (Fig. 2c and Fig. S6b). To characterize the electrostatic and hydrophobic interactions between different protein regions in this system, we constructed pairwise intermolecular interaction plots for all residue pairs between the two proteins (Fig. 7a). Our analysis revealed that TDP-43 LCD primarily interacts with the first 40 amino acids of tau's negatively charged N-terminal region. Most of the attractive electrostatic interactions occur with the positively charged N-terminal domain of TDP-43 LCD, which contains four positively charged residues within the 266–293 region. On the other hand, this domain is repelled by positively charged proline-rich and repeat domains of tau. Furthermore, the first 40 amino acids of tau are involved in hydrophobic interactions with residues throughout the TDP-43 LCD sequence, with the strongest of these mapping to the N-terminal domain of TDP-43 LCD (up to residue 293). This region contains three aromatic residues, which have a potential to engage in π-π interactions with three aromatic amino acids within the N-terminal region of tau.

Altogether, our simulations indicate that tau/TDP-43 LCD heterotypic interactions include both the electrostatic and hydrophobic forces. This is consistent with experimental data showing reduced partitioning of tau into TDP-43 LCD condensates at high salt concentrations (what suggests the importance of electrostatic interactions) as well as the persistence of tau halo around TDP-43 LCD droplets at high salt concentrations (what suggests the involvement of hydrophobic interactions) (Fig. 6a, b).

Finally, we can utilize the simulations to learn about the orientation of tau within the halo surrounding TDP-43 LCD condensates. Given that the interaction strength (represented by color intensities in Fig. 7a) reflects the

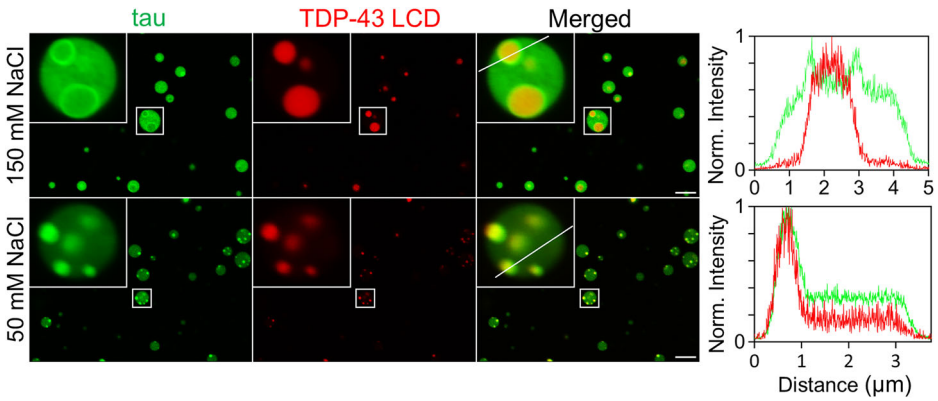

Fig. 5 | The effect of salt on tau recruitment into TDP-43 LCD droplets. Fluorescence microscopy images of mixtures containing 20 μM tau (green) and 20 μM TDP-43 LCD (red) at two different salt concentrations as indicated. Insets in the upper left corners show magnified view of selected droplets. Scale bars: 5 μm. Right panels display fluorescence intensity profiles (normalized to the maximum intensity) along the lines indicated in the corresponding merged images.

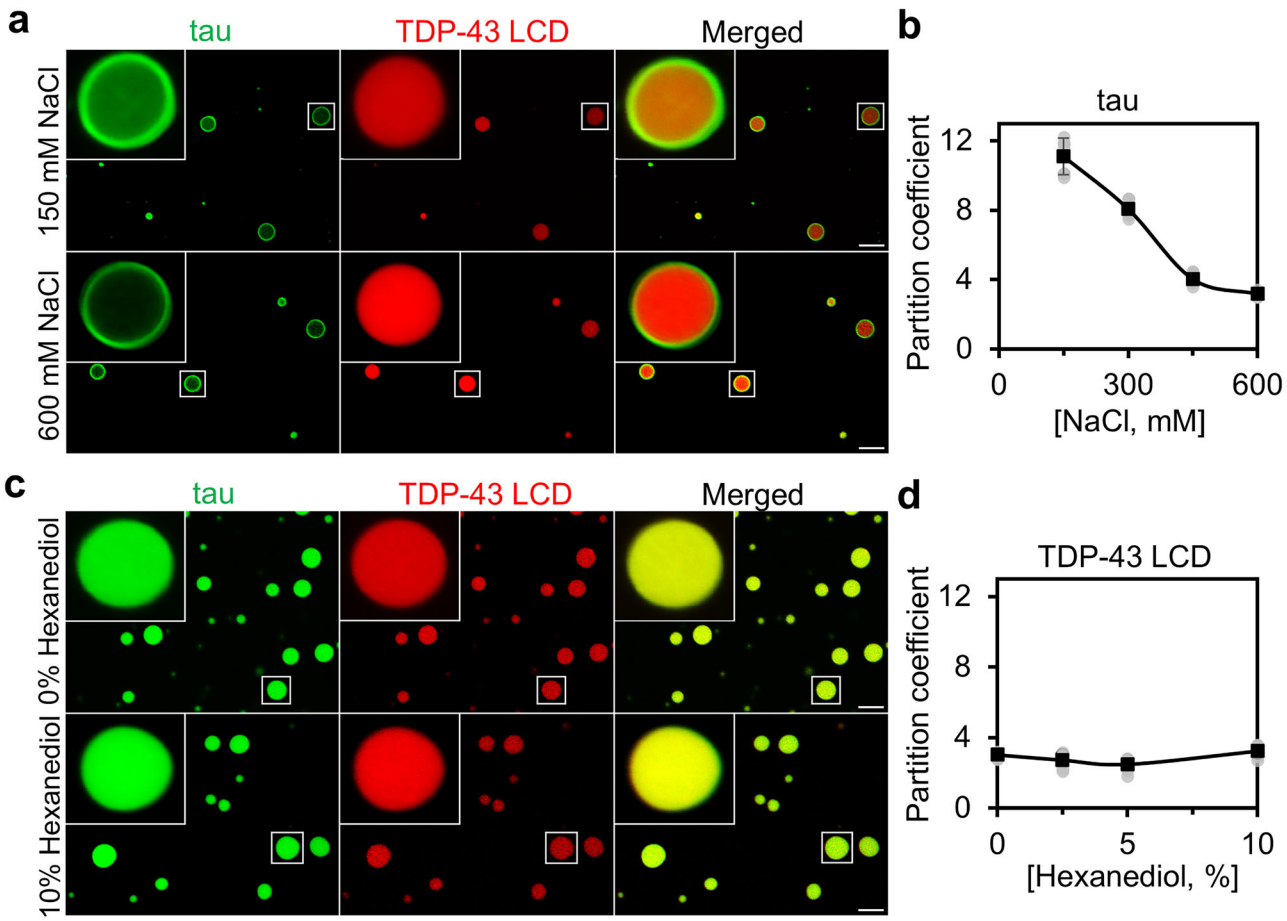

Fig. 6 | Modulation of tau/TDP-43 LCD phase behavior by salt and hexanediol. **a** Fluorescence microscopy images of mixtures containing 4 μM tau (green) and 20 μM TDP-43 LCD (red) at the indicated salt concentrations. **b** Partition coefficient of tau (4 μM) into TDP-43 LCD droplets as a function of salt concentration. **c** Fluorescence microscopy images of mixtures containing 20 μM tau (green) and 4 μM TDP-43 LCD (red) at the indicated 1,6-hexanediol concentrations. **d** Partition coefficient of TDP-43 LCD (4 μM) into tau droplets as a function of 1,6-hexanediol concentration. Gray circles show individual measurements; black squares indicate the mean, and error bars represent the standard deviation ($n = 11$). Scale bars: 5 μm.

proximity of different protein domains, our data suggest that only a small region of tau's N-terminal domain (first 40 amino acids) remains in close contact with TDP-43 LCD, where strong attractive hydrophobic and electrostatic interactions are present. In contrast, the remainder of tau appears more distant from TDP-43 LCD, consistent with weaker intermolecular interactions in these regions. This supports a model in which tau's N-terminal region binds to the TDP-43 LCD condensate surface, with the rest of the molecule extending into the dilute phase (Fig. 7b). Such an arrangement is also consistent with the observed repulsive electrostatic interactions between the positively charged N-terminal region of TDP-43 LCD and tau's proline-rich and repeat domains. To validate this hypothesis, in Fig. 7c we show radial density plots for the N-terminals (first 10 residues) of tau and TDP-43 LCD and the C-terminal (last 10 residues) of tau. Furthermore, we compared the distribution of distances between the N-terminal residue of tau and the C-terminal residue of TDP-43 LCD with that between the C-terminal residue of tau and the N-terminal residue of TDP-43 LCD (Fig. 7d). These plots confirm our hypthothesis. The radial density plots show that the peaks of both N-terminals coincide and overlap

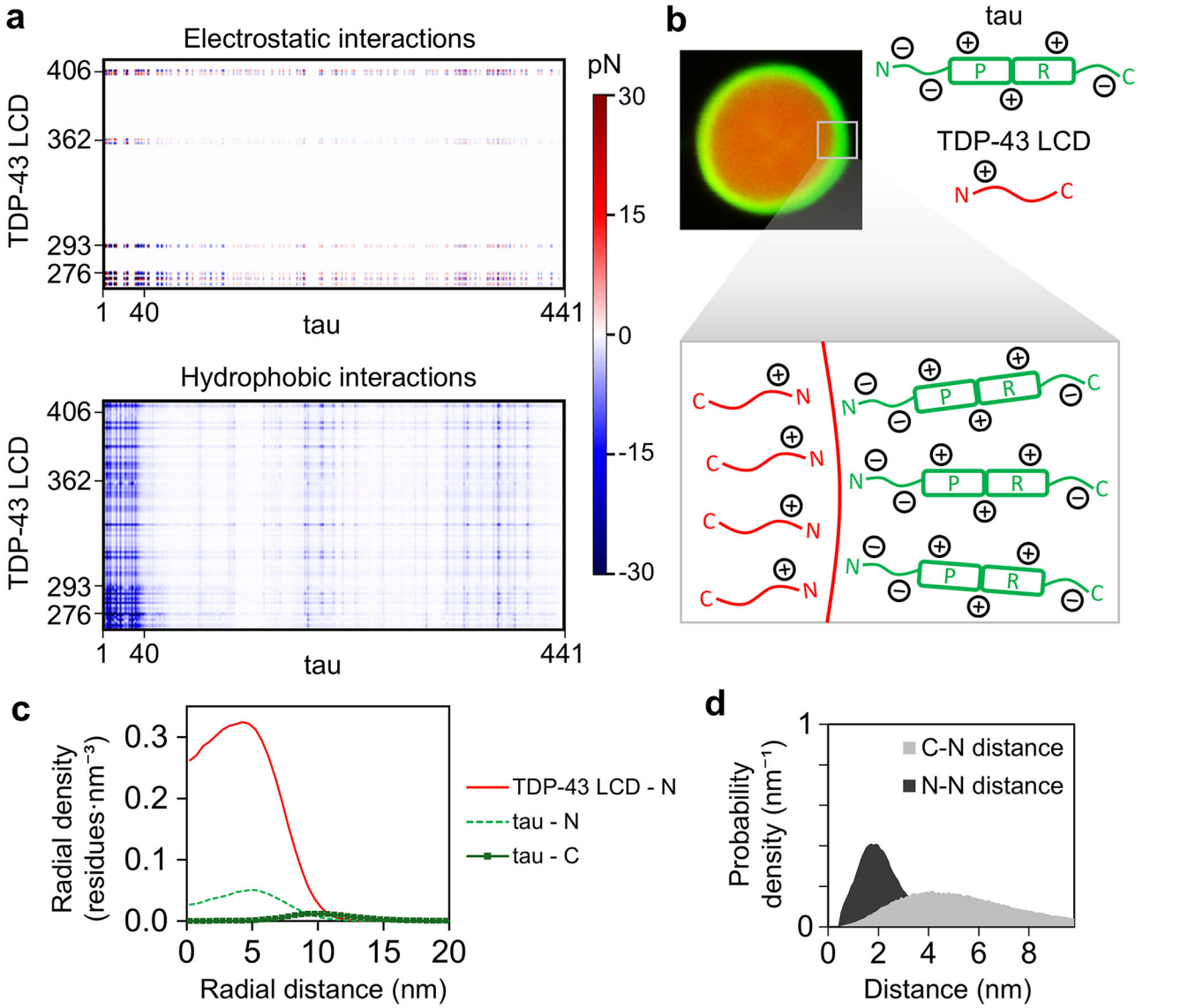

Fig. 7 | Intermolecular interactions between tau and TDP-43 LCD. Analysis of simulations in the mixture of 3 μM tau and 9 μM TDP-43 LCD. **a** Pairwise interaction plots for electrostatic (*top*) and hydrophobic (*bottom*) forces. Interaction strengths are indicated by color intensity. Attractive interactions, blue; repulsive interactions, red (scale bar: ±30 pN). **b** Schematic representation of tau halo around TDP-43 LCD droplets, highlighting electrostatic interactions between the negatively charged N-terminal region of tau and the positively charged N-terminal region of TDP-43 LCD. **c** Time-averaged radial density plots for the N-terminal (first 10 amino acids, dashed line) and C-terminal (last 10 amino acid, solid line with square markers) regions of tau (green) and the N-terminal region of TDP-43 LCD (first 10 amino acids, red solid line), normalized to give the total number of tagged amino acids when integrating over the volume of the droplet. **d** Normalized probability distributions of distances between the N-terminal residues of tau and TDP-43 LCD (N-N distance, dark gray bars) and the C-terminal residue of tau and the N-terminal residue of TDP-43 LCD (C-N distance, light gray bars).

with one another, while the C-terminal extends to larger radii. In the distances plot, the N–N distances were consistently shorter than the N-C distances, supporting the notion that interactions between tau and TDP-43 LCD are primarily mediated through their N-terminal regions.

To experimentally validate the simulation-derived prediction that tau's N-terminal region mediates its interaction with TDP-43 LCD at the condensate surface, we performed additional experiments using the tau K18 fragment (residues 244–372), which lacks both the N- and C-terminal regions. When mixed with TDP-43 LCD (20 μM), K18 (4 μM) did not form the characteristic peripheral "halo" observed for full-length tau, instead displaying a uniform distribution within TDP-43 LCD droplets (Fig. 8). These findings confirm that the negatively charged N-terminal residues of tau are critical for establishing the interfacial architecture of tau/TDP-43 LCD condensates, supporting the orientation model derived from our simulations.

Discussion

Data presented in this study show that tau and TPD-43 LCD undergo non-associative LLPS, forming immiscible condensates in which larger tau droplets envelop smaller TDP-43 LCD droplets. This immiscibility suggests relatively weak heterotypic interactions between the two proteins[17], consistent with the absence of droplet formation in the mixture containing tau and TDP-43 below their respective C_{sat}, even when their combined concentration exceeds the C_{sat} of either protein. Our findings also indicate that in multicomponent systems lacking cooperative LLPS, scaffold-client roles are determined by each protein's concentration. Thus, each protein in such a system acts as a scaffold only when its concentration exceeds C_{sat}, whereas below this threshold, it behaves as a client that is passively recruited into condensates formed by the other protein (that is above C_{sat}). Given that condensation is known to facilitate protein aggregation[7,26], such mutual co-

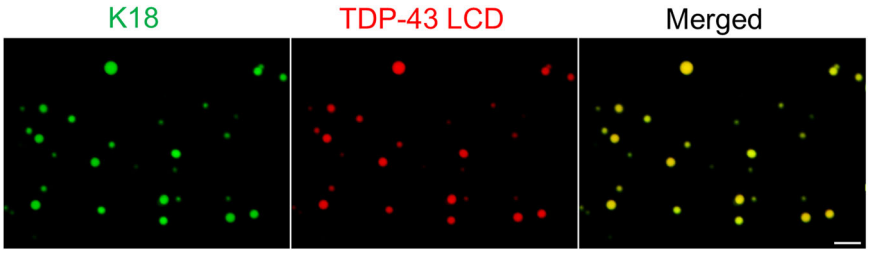

Fig. 8 | Homogeneous recruitment of the K18 tau fragment into TDP-43 LCD condensates. Fluorescence microscopy images of the mixture of K18 (green, 4 μM) and TDP-43 LCD (red, 20 μM) showing uniform colocalization of both proteins within TDP-43 LCD droplets. Scale bar: 5 μm.

recruitment of proteins into the condensed phase may contribute to synergistic pathological aggregation in vitro and in vivo.

Building on these findings, we explored whether the scaffold-client behavior of a protein mixture also depends on the strength of intermolecular interactions. While such interactions are predicted to modulate LLPS behavior in classical thermodynamic models [such as Flory-Huggins theory[1,12]] for simple polymers, direct experimental evidence of this role in protein LLPS remains very limited. Our system provides a useful model to test this prediction, as physicochemical forces underlying tau and TDP-43 LCD condensation are fundamentally distinct, allowing their selective manipulation and consequent disruption of one condensate type without affecting the other. By selectively impairing the LLPS-driving interactions of either protein, we observed a loss of scaffold function that mirrors the effect of reducing its concentration to the level below C_{sat}. These results reveal that both protein concentration and the strength of homotypic interactions govern the scaffold-client behavior in non-associative protein systems. In cells, these parameters may be modulated through transient changes in protein expression levels and/or post-translational modifications (PTMs). The latter may be particularly relevant for both tau and TDP-43 LCD, as recent data indicate that phosphorylation may significantly alter the LLPS propensity of both proteins[38,41,46,47]. PTMs may also influence heterotypic interactions. However, such effects depend on whether PTM sites lie within regions that mediate these interactions, and are therefore highly context-specific. For example, the major phosphorylation sites of tau and TDP-43 LCD are located outside the N-terminal regions that drive interactions between these two proteins, making this system not well suited for exploring the role of PTMs in modulating heterotypic interactions.

Apart from shedding new light into the scaffold-client behavior in multicomponent protein systems, our data also provided insights into the principles governing the architecture of multiphasic condensates. The multiphasic organization observed here for tau/TDP-43 LCD mixtures resembles the behavior reported for other protein systems in vitro[48,49] as well for cellular compartments such as P granules[2], stress granules[50], or nucleoli[51]. Such stratification is thought to arise from differences in surface tension, with condensates of higher surface tension positioning at the core of droplets with greater solvent affinity[19,20]. Our findings not only provide further verification of this model but also offer a molecular-level insight into the capillary forces that control the organization of multiphase condensates. Specifically, we found that interfacial tension between tau and TDP-43 LCD condensates can be modulated by the strength of their heterotypic interactions. At low salt concentrations, TDP-43 LCD droplets embedded within tau condensates become smaller and more numerous, reflecting reduced surface tensions and lower fusion propensity. This effect correlates with an enhanced tau recruitment into TDP-43 LCD condensates at low ionic strength, indicating stronger tau-TDP-43 LCD interactions. This is consistent with the electrostatic nature of these interactions that was revealed in our simulations. Altogether, these findings highlight the role of heterotypic interactions between scaffolds in determining the architecture of multiphasic condensates.

Our findings also provide mechanistic insight into the striking feature of tau/TDP-43 LCD mixtures: the formation of a tau-rich "halo" at the surface of TDP-43 LCD condensates. A somewhat similar shell-like organization has been reported for systems such as Lge1/Bre1[52] and TDP-43/Hsp70[53]. However, little is known about the nature of interactions responsible for these types of morphologies. In an effort to bridge this gap, we first examined the chemical nature of tau/TDP-43 LCD interactions experimentally. Although their salt sensitivity suggests an electrostatic component, the persistence of the tau halo at high ionic strength indicates additional stabilization by hydrophobic forces. To dissect these contributions, we utilized a sequence-dependent coarse-grained simulation model. Our simulations recapitulated the observed phase behavior and spatial organization of tau/TDP-43 LCD mixtures, revealing that residues 1-40 of tau's negatively charged N-terminus interact primarily with the positively charged N-terminal region of TDP-43 LCD through a combination of electrostatic and hydrophobic forces. Importantly, in silico data also suggested that tau at the droplet interface adopts a specific configuration in which its N-terminal region remains in close contact with TDP-43 LCD molecules inside the condensates, while its positively charged domains are repelled by similarly charged regions of TDP-43 LCD, becoming exposed to the aqueous phase (Fig. 7b). This prediction was experimentally validated using tau K18 fragment that did not form the characteristic halo around TDP-43 LCD condensates (Fig. 8), confirming the critical role of N-terminal residues in full-length tau in establishing this interfacial organization.

The formation of tau halo around TDP-43 LCD droplets is reminiscent of the core-shell organization observed in layered coacervates of elastin-like polypeptides (ELPs), where amphiphilic diblock ELPs accumulate at the surface of hydrophobic monoblock ELP droplets[54]. Given tau's substantially greater hydrophilicity relative to TDP-43 LCD, N-terminal interactions between the two proteins generate an amphiphilic assembly with a preferred orientation: the hydrophobic TDP-43 LCD region localizes toward the droplet core, while the hydrophilic tau segment remains exposed to the aqueous phase (Fig. 7b). In TDP-43 LCD droplets enveloped by tau condensates, tau likely adopts a similar orientation within the halo formed at the interface between the two condensates, with its N-terminal region directed toward TDP-43 LCD droplets and the remaining domains extending outward to interact with tau molecules in the surrounding condensate. This arrangement mirrors the behavior described for amphiphilic guest molecules in model multicomponent coacervates, where such molecules preferentially localize at the interface between hydrophobic inner droplets and hydrophilic outer phases[55]. Thus, our results support a notion that proteins of contrasting hydrophobicities can associate to form amphiphilic complexes that are enriched at condensate surfaces.

These findings indicate that halo formation is governed by the same interfacial tension principles that underlie the organization of multiphasic condensates. Thus, when TDP-43 LCD condensates are dispersed in aqueous solution, tau accumulates at their interfaces to reduce unfavorable TDP-43 LCD-water interactions, thereby minimizing surface tension. Similarly, when TDP-43 LCD droplets are encapsulated within tau condensates, tau-tau interactions at the interface offset the energetic penalty of tau-TDP-43 LCD contacts. Together, these observations suggest a unifying model in which minimization of interfacial tension drives surface accumulation of amphiphilic assemblies, an organizing principle that may apply to diverse multicomponent condensates.

Methods

Protein expression, purification, and labeling

Recombinant TDP-43 LCD (residues 266–414) was expressed, purified, treated with thrombin protease (to remove the His tag) and refolded as previously described[41]. Prior to experiments, lyophilized TDP-43 LCD was resuspended in Milli-Q water and filtered using100 kDa Amicon centrifugal filter. Protein concentration was determined spectrophotometrically (mass extinction coefficient 17990 $M^{-1}.cm^{-1}$). Alexa Fluor 594-labeled or Alexa Fluor 488-labeled TDP-43 LCD was prepared as described previously[41].

Recombinant full-length tau (residues 1-441) and the K18 fragment (residues 244-372) were expressed and purified using a previously described protocol[33]. When necessary, a second size-exclusion chromatography (Superdex 75 10/300 GL column) step was performed to ensure purify, which was assessed by PAGE and UV absorbance spectroscopy (Nanodrop). Protein concentration was determined using the reducing-agent–compatible BCA assay (Thermo Fisher Scientific). Tau variants were labeled with Alexa Fluor 488 (Invitrogen) as described previously[33].

The amino acid sequences of all recombinant proteins used in this study (TDP-43 LCD, tau, and K18) are provided in Supplementary Table S1. Protein purity was assessed by SDS–PAGE followed by Coomassie Blue staining. A representative gel is shown in Fig. S4. Densitometric analysis performed in ImageJ indicated purities of 100% for TDP-43 LCD, 93% for tau, and 91% for K18. The plasmids encoding the proteins used in this study are available from the corresponding author W.K.S. upon request.

Liquid-liquid phase separation (LLPS) assays

LLPS was evaluated by turbidity measurements and fluorescence microscopy at room temperature. All experiments were conducted in 10 mM HEPES buffer (pH 7.4) containing 10% polyethylene glycol (PEG; 10.000 kDa), 1 mM EDTA, and 1 mM DTT. For the experiment with fluorescent-labeled PEG, unlabeled PEG was mixed with FITC-labeled PEG (5 kDa, Creative PEGWorks) at a 1:4 ratio. All solutions were freshly prepared for each experiment. To ensure reproducibility, all assays were performed with a minimum of four experimental replicates and two independent protein purification batches.

Turbidity was quantified as optical density at 600 nm using Tecan Spark multimode microplate reader. Droplets were visualized by fluorescence microscopy using AlexaFluor-labeled protein probes (0.2 μM) mixed with the unlabeled protein at a desired concentration. Samples (20 μL) were placed onto 35 mm glass-bottom dishes pre-coated with Pluronic® F-127 to minimize surface adhesion and sealed with a cover glass to avoid evaporation. Imaging was performed on an Olympus FV3000 confocal microscope using a X60 oil-immersion objective, 1080 ×1080 resolution, and 2X zoom. Excitation lasers at 488 nm and 561 nm were used to detect Alexa Fluor 488-labeled tau and Alexa Fluor 594-labeled TPD-43 LCD, respectively. Laser power was optimized independently for each experimental condition to ensure adequate visualization of condensate morphology while avoiding pixel oversaturation. Images were acquired from the bottom of the dish, 15 minutes after sample preparation, to allow for droplet sedimentation. Wetting behavior was evaluated on uncoated glass surfaces to mimic a polar aqueous environment. Z-stacks were acquired for condensates sedimented at the bottom of the dish using 0.25 μm step intervals.

Images were processed in Fiji (ImageJ version 1.53 u). Scale bars (5 μm) were added, and fluorescence intensity profiles were obtained using the "Plot Profile" functionality. For visualization of relative protein distribution within condensates, fluorescence intensity values were normalized within each profile by dividing all values by the maximum intensity in that profile. Interfacial angles were measured using Angle Tool in orthogonal views reconstructed from Z-stack images, with the vertex placed at the condensate-glass contact line. Partition coefficients were calculated as the ratio of mean fluorescence intensity inside versus that outside the condensates. For evaluating the proportion of tau condensates containing TDP-43 LCD, we determined the regions of interest (ROIs) corresponding to each tau condensate using the Otsu thresholding method in Fiji (Fig. S2). Mean fluorescence intensities on the TDP-43 LCD (red) channel were measured within each ROI, corresponding to the average pixel intensity within that condensate. To determine background signal for this channel, mean intensities were measured in 14 ROIs drawn outside tau condensates, providing background mean (μ_{BG}) and standard deviation (σ_{BG}) values. A condensate was classified as heterotypic when its mean TDP-43 LCD fluorescence intensity within tau condensate exceeded the threshold defined as $\mu_{BG} + 3\times\sigma_{BG}$.

FRAP experiments

Samples for FRAP were prepared as described above for fluorescence microscopy imaging. In experiments involving mixtures of the two proteins, only the protein for which the fluorescence recovery was being determined was labeled. Droplets were allowed to sediment at the bottom of a 35 mm dish for 15 min prior to imaging. FRAP measurements were performed using a Leica HyVolution SP8 confocal microscope with 2.4 mW laser intensity for bleaching, ×63/1.4 numerical aperture oil-immersion objective, and photomultiplier tube detector. The regions of interest (0.4 μm diameter) were bleached within the droplets. The measurements involved three pre-bleaching frames, four flashes of bleaching (25% of laser power), and 70 post-bleaching frames (1.3 s/frame). Individual FRAP traces were normalized to account for background fluorescence, acquisition-related photobleaching, and pre-bleach intensity, following established workflows for quantitative FRAP analysis[56]. The mean normalized curve with the standard deviation was plotted.

Coarse-grained simulation framework and workflow

A variety of coarse-grained molecular dynamic simulation frameworks have been developed over the years to study different aspects of the dynamics and phase behavior of intrinsically disordered proteins[41,57–63]. In these models, amino acids are represented as soft spheres with defined mass, charge, and size, with harmonic springs for bonds, and non-bonded interactions approximated as sums of electrostatic and non-ionic interactions. Some studies have used Debye–Hückel potentials to model the screened electrostatic interactions with modified Lennard-Jones potentials of the Ashbaugh-Hatch functional form[64] and hydrophobicity parameters (λ) that determine the strength of non-ionic interactions[41,57–59,61]. Other classes of models, such as Mpipi models, have introduced the Wang-Frenkel potential for non-ionic interactions while still utilizing Debye-Hückel potentials for electrostatics in various forms[60,62].

In our simulations, electrostatic interactions were computed for particle pairs within 3.5 nm using a Debye–Hückel potential with a screening length of $\lambda_D = 0.7466$ nm. For non-ionic interactions, three candidate models were considered in our study. Two of them used the Ashbaugh-Hatch functional form[64], where in one case, the λ values were derived from the Kapcha-Rossky scale[65], and in the other from the Urry[66] scale (Table S1). The third model tested was the Mpipi[60] with the Wang-Frenkel potential. Among these, only the Mpipi model successfully reproduced the previously reported higher LLPS propensity of TDP-43 LCD relative to tau in the absence of crowding agents [in contrast to TDP-43 LCD[31], tau at concentrations used in the present study does not undergo LLPS without molecular crowders[33]]. This is likely due to more refined parametrization of intermolecular interactions in the Mpipi model. Therefore, the Mpipi model with modifications was used for all simulations presented in this study. Additional Mpipi model details, including functional forms for potentials/forces, are provided in the Supplementary Methods.

All simulations were carried out in the presence of 1 mM EDTA, 10 mM HEPES, and 150 mM NaCl. EDTA and HEPES were modeled implicitly by incorporating the ionic strength of their dissociated species into the Debye screening length. To account for the LLPS-enhancing effects of PEG, electrostatic and non-ionic interactions in the Mpipi model were scaled using two empirical constants, α and β, respectively. Although explicit inclusion of PEG would allow direct interaction with proteins, the resulting increase in system size would require further coarse-graining to remain computationally feasible — an approach avoided to preserve the level of molecular detail required for meaningful structural analysis. Instead, scaling

parameters were calibrated by simulating each individual protein at 5 μM, near the experimentally determined saturation concentrations of tau and TDP-43 LCD (4.9 μM & 4.8 μM, respectively) in 10% PEG (Fig. 1a). Individual systems of tau and TDP-43 LCD first formed droplets at $\alpha = 3.115$ and $\beta = 1.315$ in simulations. Thus, these global scaling parameters were tuned such that the concentration at which the simulated proteins underwent LLPS was roughly the same as experiment. These scaling parameters were then kept the same for all simulations of tau and TDP-43 LCD mixtures.

Simulations were performed using the Python-based molecular dynamic toolkit HOOMD-Blue[67,68]. The simulation box was a slab configuration (200 x 200 x 600 nm), with periodic boundary conditions, a setup often used in intrinsically disordered protein simulations[57–59,61,63]. The time evolution of the system was simulated using Langevin dynamics, using a time step of 0.01 ps. Simulations were run for either 2 or 5 μs, depending on whether they were used for single-protein or protein mixture systems, respectively. In both cases, the first 1 μs was allocated for equilibration and the remaining time was used for analysis. Extra details of simulation procedures can be found in the Supplementary Methods.

Simulation analysis procedures

To assess whether phase separation occurred, we developed a protocol to detect microdroplet formation — smaller assemblies than the large condensates typically seen in experiments, which are not reproducible in silico due to limited system size and simulation timescales. Proteins whose centers of mass were within a 10 nm radius of each other were considered part of the same cluster. A system was classified as phase-separated if the average cluster size per protein exceeded two throughout all post-equilibration time steps, although the classification was not strongly dependant on the precise value of this cutoff.

To quantify spatial distribution of proteins within mixed condensates, we simulated fluorescence labeling in the experiment by tagging all lysines and N-termini in each protein. At each post-equilibration time step, the largest protein cluster was identified, and the positions of all amino acids were translated along the x-, y-, and z-axes to center the cluster's center of mass in simulation box. Radial shells were created eminating from the center of mass of the largest cluster, and radial densities of tagged amino acids were calculated for each shell. These densities were normalized such that integrating over the whole volume will give the total number of tagged amino acids. To check whether the simulation box dimensions had any effect on the qualitative results, a single simulation was conducted with TDP-43 LCD at 9 μM and tau at 3 μM in a cubic simulation box (346x346x346 nm) with all parameters the same as the slab simulation. Radial distributions of both proteins were generated for this simulation in the same way as the slab simulations, and the radial profiles were compared (Fig. S6), showing the same qualitative features in both cases, up to stochastic fluctuations in droplet size between simulation runs. The lack of dependence on boundary conditions is expected, since the smallest dimension of the simulation box in both slab and cubic cases is larger than the radii of the biggest droplet.

To evaluate spatial orientation of tau relative to TDP-43 LCD condensates in simulations at 3 μM tau and 9 μM TDP-43 LCD, we quantified the positions of tau's N- and C-terminal residues at each post-equilibration time step and calculated their distances to the nearest TDP-43 LCD N-terminal. Only distances <10 nm were included to exclude contributions from unbound or dilute-phase proteins. This analysis generated two distributions of distances, tau N-terminus to TDP-43 LCD N-terminus (N–N) and tau C-terminus to TDP-43 LCD N-terminus (C–N), used to assess preferential domain interactions (Fig. 6d). Furthermore, radial density plots were created for tau and TDP-43 LCD 10 N-terminal residues and tau 10 C-terminal residues.

Reporting summary

Further information on research design is available in the Nature Portfolio Reporting Summary linked to this article.

Data availability

Data supporting the findings of this study are available within the paper, its Supplementary Information, Supplementary Data 1–2, and in public repositories at Zenodo (https://doi.org/10.5281/zenodo.18370808; source data) and the Open Science Framework (https://doi.org/10.17605/OSF.IO/4VMQB; simulation datasets).

Code availability

The custom code used to perform all coarse-grained simulations and analysis is available at: https://doi.org/10.5281/zenodo.15680574.

Received: 30 June 2025; Accepted: 28 January 2026;
Published online: 11 February 2026

References

1. Flory, P. J. Thermodynamics of high polymer solutions. *J. Chem. Phys.* **10**, 51–61 (1942).
2. Brangwynne, C. P. et al. Germline P granules are liquid droplets that localize by controlled dissolution/condensation. *Science* **324**, 1729–1732 (2009).
3. Mitrea, D. M. & Kriwacki, R. W. Phase separation in biology; functional organization of a higher order. *Cell Commun. Signal. CCS* **14**, 1 (2016).
4. Shin, Y. & Brangwynne, C. P. Liquid phase condensation in cell physiology and disease. *Science* **357**, eaaf4382 (2017).
5. Banani, S. F., Lee, H. O., Hyman, A. A. & Rosen, M. K. Biomolecular condensates: organizers of cellular biochemistry. *Nat. Rev. Mol. Cell Biol.* **18**, 285–298 (2017).
6. Uversky, V. N. Intrinsically disordered proteins in overcrowded milieu: Membrane-less organelles, phase separation, and intrinsic disorder. *Curr. Opin. Struct. Biol.* **44**, 18–30 (2017).
7. Babinchak, W. M. & Surewicz, W. K. Liquid-liquid phase separation and its mechanistic role in pathological protein aggregation. *J. Mol. Biol.* **432**, 1910–1925 (2020).
8. Boyko, S. & Surewicz, W. K. Tau liquid-liquid phase separation in neurodegenerative diseases. *Trends Cell Biol.* **32**, 611–623 (2022).
9. Zbinden, A., Pérez-Berlanga, M., De Rossi, P. & Polymenidou, M. Phase separation and neurodegenerative diseases: a disturbance in the force. *Dev. Cell* **55**, 45–68 (2020).
10. Boeynaems, S. et al. Protein phase separation: a new phase in cell biology. *Trends Cell Biol.* **28**, 420–435 (2018).
11. Pak, C. W. et al. Sequence determinants of intracellular phase separation by complex coacervation of a disordered protein. *Mol. Cell* **63**, 72–85 (2016).
12. Brangwynne, C. P., Tompa, P. & Pappu, R. V. Polymer physics of intracellular phase transitions. *Nat. Phys.* **11**, 899–904 (2015).
13. Oldfield, C. J. & Dunker, A. K. Intrinsically disordered proteins and intrinsically disordered protein regions. *Annu. Rev. Biochem.* **83**, 553–584 (2014).
14. Banani, S. F. et al. Compositional control of phase-separated cellular bodies. *Cell* **166**, 651–663 (2016).
15. Sanchez-Burgos, I., Espinosa, J. R., Joseph, J. A. & Collepardo-Guevara, R. Valency and binding affinity variations can regulate the multilayered organization of protein condensates with many components. *Biomolecules* **11**, 278 (2021).
16. Joseph, J. A. et al. Thermodynamics and kinetics of phase separation of protein-RNA mixtures by a minimal model. *Biophys. J.* **120**, 1219–1230 (2021).
17. Ribeiro, S. S., Samanta, N., Ebbinghaus, S. & Marcos, J. C. The synergic effect of water and biomolecules in intracellular phase separation. *Nat. Rev. Chem.* **3**, 552–561 (2019).

18. Espinosa, J. R. et al. Liquid network connectivity regulates the stability and composition of biomolecular condensates with many components. *Proc. Natl. Acad. Sci. USA* **117**, 13238–13247 (2020).
19. Gouveia, B. et al. Capillary forces generated by biomolecular condensates. *Nature* **609**, 255–264 (2022).
20. Ye, S. et al. Micropolarity governs the structural organization of biomolecular condensates. *Nat. Chem. Biol.* **20**, 443–451 (2024).
21. Feric, M. et al. Coexisting liquid phases underlie nucleolar subcompartments. *Cell* **165**, 1686–1697 (2016).
22. Ghosh, A., Zhang, X. & Zhou, H.-X. Tug of war between condensate phases in a minimal macromolecular system. *J. Am. Chem. Soc.* **142**, 8848–8861 (2020).
23. Wheeler, J. R., Matheny, T., Jain, S., Abrisch, R. & Parker, R. Distinct stages in stress granule assembly and disassembly. *eLife* **5**, e18413 (2016).
24. Molliex, A. et al. Phase separation by low complexity domains promotes stress granule assembly and drives pathological fibrillization. *Cell* **163**, 123–133 (2015).
25. Murakami, T. et al. ALS/FTD mutation-induced phase transition of FUS liquid droplets and reversible hydrogels into irreversible hydrogels impairs RNP granule function. *Neuron* **88**, 678–690 (2015).
26. Patel, A. et al. A liquid-to-solid phase transition of the ALS protein FUS accelerated by disease mutation. *Cell* **162**, 1066–1077 (2015).
27. Galpern, W. R. & Lang, A. E. Interface between tauopathies and synucleinopathies: a tale of two proteins. *Ann. Neurol.* **59**, 449–458 (2006).
28. Smith, V. D. et al. Overlapping but distinct TDP-43 and tau pathologic patterns in aged hippocampi. *Brain Pathol. Zur. Switz.* **28**, 264–273 (2018).
29. Higashi, S. et al. Concurrence of TDP-43, tau and alpha-synuclein pathology in brains of Alzheimer's disease and dementia with Lewy bodies. *Brain Res.* **1184**, 284–294 (2007).
30. Jack, C. R. J. Advances in Alzheimer's disease research over the past two decades. *Lancet Neurol.* **21**, 866–869 (2022).
31. Babinchak, W. M. et al. The role of liquid-liquid phase separation in aggregation of the TDP-43 low-complexity domain. *J. Biol. Chem.* **294**, 6306–6317 (2019).
32. Conicella, A. E. et al. TDP-43 α-helical structure tunes liquid-liquid phase separation and function. *Proc. Natl. Acad. Sci. USA* **117**, 5883–5894 (2020).
33. Boyko, S., Qi, X., Chen, T.-H., Surewicz, K. & Surewicz, W. K. Liquid-liquid phase separation of tau protein: The crucial role of electrostatic interactions. *J. Biol. Chem.* **294**, 11054–11059 (2019).
34. Conicella, A. E., Zerze, G. H., Mittal, J. & Fawzi, N. L. ALS mutations disrupt phase separation mediated by α-helical structure in the TDP-43 low-complexity C-terminal domain. *Struct. Lond. Engl. 1993* **24**, 1537–1549 (2016).
35. Li, H.-R., Chiang, W.-C., Chou, P.-C., Wang, W.-J. & Huang, J.-R. TAR DNA-binding protein 43 (TDP-43) liquid-liquid phase separation is mediated by just a few aromatic residues. *J. Biol. Chem.* **293**, 6090–6098 (2018).
36. Alberti, S., Gladfelter, A. & Mittag, T. Considerations and Challenges in Studying Liquid-Liquid Phase Separation and Biomolecular Condensates. *Cell* **176**, 419–434 (2019).
37. Boyko, S., Surewicz, K. & Surewicz, W. K. Regulatory mechanisms of tau protein fibrillation under the conditions of liquid-liquid phase separation. *Proc. Natl. Acad. Sci. Usa.* **117**, 31882–31890 (2020).
38. Boyko, S. & Surewicz, W. K. Domain-specific modulatory effects of phosphomimetic substitutions on liquid-liquid phase separation of tau protein. *J. Biol. Chem*. **299**, 104722 (2023).
39. McGurk, L. et al. Poly(ADP-Ribose) prevents pathological phase separation of TDP-43 by promoting liquid demixing and stress granule localization. *Mol. Cell* **71**, 703–717.e9 (2018).
40. Espejo, N. H. et al. Compositional control of ageing kinetics in TDP-43 condensates. *PRX Life* **3**, 043018 (2025).
41. Haider, R., Shipley, B., Surewicz, K., Hinczewski, M. & Surewicz, W. K. Pathological C-terminal phosphomimetic substitutions alter the mechanism of liquid-liquid phase separation of TDP-43 low complexity domain. *Protein Sci. Publ. Protein Soc.* **33**, e5179 (2024).
42. Haider, R., Penumutchu, S., Boyko, S. & Surewicz, W. K. Phosphomimetic substitutions in TDP-43's transiently α-helical region suppress phase separation. *Biophys. J.* **123**, 361–373 (2024).
43. Chauhan, G., Bremer, A., Dar, F., Mittag, T. & Pappu, R. V. Crowder titrations enable the quantification of driving forces for macromolecular phase separation. *Biophys. J.* **123**, 1376–1392 (2024).
44. Düster, R., Kaltheuner, I. H., Schmitz, M. & Geyer, M. 1,6-Hexanediol, commonly used to dissolve liquid-liquid phase separated condensates, directly impairs kinase and phosphatase activities. *J. Biol. Chem.* **296**, 100260 (2021).
45. Ribbeck, K. & Görlich, D. The permeability barrier of nuclear pore complexes appears to operate via hydrophobic exclusion. *EMBO J.* **21**, 2664–2671 (2002).
46. Savastano, A. et al. Disease-Associated Tau Phosphorylation Hinders Tubulin Assembly within Tau Condensates. *Angew. Chem. Int. Ed. Engl.* **60**, 726–730 (2021).
47. Gruijs da Silva, L. A. et al. Disease-linked TDP-43 hyperphosphorylation suppresses TDP-43 condensation and aggregation. *EMBO J.* **41**, e108443 (2022).
48. Sawyer, I. A., Sturgill, D. & Dundr, M. Membraneless nuclear organelles and the search for phases within phases. *WIREs RNA* **10**, e1514 (2019).
49. Choi, S., Meyer, M. O., Bevilacqua, P. C. & Keating, C. D. Phase-specific RNA accumulation and duplex thermodynamics in multiphase coacervate models for membraneless organelles. *Nat. Chem.* **14**, 1110–1117 (2022).
50. Protter, D. S. W. & Parker, R. Principles and properties of stress granules. *Trends Cell Biol.* **26**, 668–679 (2016).
51. Lafontaine, D. L. J., Riback, J. A., Bascetin, R. & Brangwynne, C. P. The nucleolus as a multiphase liquid condensate. *Nat. Rev. Mol. Cell Biol.* **22**, 165–182 (2021).
52. Gallego, L. D. et al. Phase separation directs ubiquitination of gene-body nucleosomes. *Nature* **579**, 592–597 (2020).
53. Yu, H. et al. HSP70 chaperones RNA-free TDP-43 into anisotropic intranuclear liquid spherical shells. *Science* **371**, eabb4309 (2021).
54. Simon, J. R., Carroll, N. J., Rubinstein, M., Chilkoti, A. & López, G. P. Programming molecular self-assembly of intrinsically disordered proteins containing sequences of low complexity. *Nat. Chem.* **9**, 509–515 (2017).
55. Lu, T. & Spruijt, E. Multiphase complex coacervate droplets. *J. Am. Chem. Soc.* **142**, 2905–2914 (2020).
56. Kang, M., Andreani, M. & Kenworthy, A. K. Validation of normalizations, scaling, and photofading corrections for FRAP data analysis. *PloS One* **10**, e0127966 (2015).
57. Mammen Regy, R., Zheng, W. & Mittal, J. Using a sequence-specific coarse-grained model for studying protein liquid-liquid phase separation. *Methods Enzymol.* **646**, 1–17 (2021).
58. Regy, R. M., Thompson, J., Kim, Y. C. & Mittal, J. Improved coarse-grained model for studying sequence dependent phase separation of disordered proteins. *Protein Sci.* **30**, 1371–1379 (2021).
59. Dignon, G. L., Zheng, W., Kim, Y. C., Best, R. B. & Mittal, J. Sequence determinants of protein phase behavior from a coarse-grained model. *PLoS Comput. Biol.* **14**, e1005941 (2018).
60. Joseph, J. A. et al. Physics-driven coarse-grained model for biomolecular phase separation with near-quantitative accuracy. *Nat. Comput. Sci.* **1**, 732–743 (2021).
61. Tesei, G. & Lindorff-Larsen, K. Improved predictions of phase behaviour of intrinsically disordered proteins by tuning the interaction range. *Open Res. Eur.* **2**, 94 (2022).

62. Tejedor, A. et al. Chemically Informed Coarse-Graining of Electrostatic Forces in Charge-Rich Biomolecular Condensates. *ACS Cent. Sci.* **11**, 302–321 (2025).
63. Dignon, G. L., Zheng, W., Best, R. B., Kim, Y. C. & Mittal, J. Relation between single-molecule properties and phase behavior of intrinsically disordered proteins. *Proc. Natl. Acad. Sci. USA* **115**, 9929–9934 (2018).
64. Ashbaugh, H. S. & Hatch, H. W. Natively unfolded protein stability as a coil-to-globule transition in charge/hydropathy space. *J. Am. Chem. Soc.* **130**, 9536–9542 (2008).
65. Kapcha, L. H. & Rossky, P. J. A simple atomic-level hydrophobicity scale reveals protein interfacial structure. *J. Mol. Biol.* **426**, 484–498 (2014).
66. Urry, D. W. et al. Hydrophobicity scale for proteins based on inverse temperature transitions. *Biopolymers* **32**, 1243–1250 (1992).
67. Howard, M. P., Panagiotopoulos, A. Z. & Nikoubashman, A. Efficient mesoscale hydrodynamics: Multiparticle collision dynamics with massively parallel GPU acceleration. *Comput. Phys. Commun.* **230**, 10–20 (2018).
68. Anderson, J. A., Glaser, J. & Glotzer, S. C. HOOMD-blue: A Python package for high-performance molecular dynamics and hard particle Monte Carlo simulations. *Comput. Mater. Sci.* **173**, 109363 (2020).

Acknowledgements

We thank Raza Haider for assistance with TDP-43 LCD purification. This work was supported by the National Institutes of health grants R21 AG094047 and RF1 AG061797 awarded to W.K.S. The content is solely the responsibility of the authors and does not necessarily represent the official views of the National Institutes of Health. V.U.M. is supported by *Marcos Lottenberg & Marcus Wolosker International Fellowship for Physicians Scientist - Case Western*.

Author contributions

Conceptualization: V.U.M., W.K.S. Methodology: V.U.M., W.K.S. (in vitro experiments); B.S., M.H. (in silico simulations). Investigation: V.U.M., S.B. (in vitro experiments); B.S. (in silico simulations). Formal analysis: V.U.M., S.B. (in vitro experiments); B.S. (in silico simulations). Writing—original draft: V.U.M., W.K.S.; B.S., M.H. (simulation-related sections). Writing—review & editing: V.U.M., W.K.S., S.B., B.S., M.H., P.M.C.A. Supervision: W.K.S., M.H., P.M.C.A. Project administration: P.M.C.A.

Competing interests

The authors declare no competing interests.

Additional information

Supplementary information The online version contains supplementary material available at https://doi.org/10.1038/s42004-026-01933-8.

Correspondence and requests for materials should be addressed to Michael Hinczewski or Witold K. Surewicz.

Peer review information *Communications Chemistry* thanks the anonymous reviewers for their contribution to the peer review of this work.